Dicarboxylated hyaluronate: Synthesis of a new, highly functionalized and biocompatible derivative

Dicarboxylated Hyaluronate: Synthesis of a New, Highly Functionalized and Biocompatible Derivative

Lukáš Münster[*1], Zdenka Capáková[1], Petr Humpolíček[1], Ivo Kuřitka[1], Bjørn E. Christensen[2], Jan Vícha[1]*

[1]Centre of Polymer Systems, Tomas Bata University in Zlín, tř. Tomáše Bati 5678, 760 01 Zlín, Czech Republic

[2]NOBIPOL, Department of Biotechnology and Food Science, Norwegian University of Science and Technology (NTNU), Trondheim, Norway

Email: munster@utb.cz

Abstract

Sequential periodate-chlorite oxidation of sodium hyaluronate to 2,3-dicarboxylated hyaluronate (DCH), a novel biocompatible and highly functionalized derivative bearing additional pair of –COOH groups at C2 and C3 carbons of oxidized D-glucuronic acid units, is investigated. The impact of various reaction parameters (time, oxidizer concentration, and molar amount) on DCH's composition, molecular weight, degree of oxidation, and cytotoxicity are investigated to guide the synthesis of DCH derivatives of desired properties. Subsequently, fully (99%) and partially (70%) oxidized DCH derivatives were compared to untreated sodium hyaluronate in terms of anticancer drug cisplatin loading efficacy, carrier capacity, drug release rates, and cytotoxicity towards healthy and cancerous cell lines. DCH derivatives were found to be superior in every aspect, having nearly twice the carrier capacity, significantly slower release rates, and higher efficacy. DCH is thus a highly interesting hyaluronate derivative with an adjustable degree of oxidation, molecular weight, and great potential for further modifications.

Keywords: sodium hyaluronate; selective oxidation; periodate oxidation; chlorite oxidation; dicarboxylated hyaluronate; cisplatin;

1. Introduction

The development of state-of-the-art biomedical materials and drug delivery systems is often closely bound to polysaccharides and their derivatives. The main motive behind their utilization is their physicochemical and physiological properties, namely good biodegradability, biocompatibility, and low immunogenicity. (Metaxa et al., 2021; Prasher et al., 2021) Moreover, various therapeutic drugs can be conjugated with polysaccharides, forming various drug delivery systems with a tunable and stimuli-responsive release. (Marchessault et al., 2006; Sharma et al., 2020) Among the myriad of polysaccharides, hyaluronic acid (HYA), a linear glycosaminoglycan (heteroglycan) composed of D-glucuronic acid (GlcA) and N-acetyl-D-glucosamine (GlcNAc) units linked *via* alternating β-(1→3) and β-(1→4) glycosidic bonds, is one of the most prospective candidates for biomedical applications, having excellent biocompatibility and biodegradability, and non-inflammatory, non-toxicity, and non-immunogenic behavior. (Balazs, 1992; Bayer, 2020; Laurent, 1998) HYA is present in bacteria and vertebrates, where its high-molecular-weight macromolecules play an important structural and hydration role in the extracellular matrix (ECM), synovial fluid, cartilages, muscular connective tissues, or the vitreous body of the eye and where it mediates various biological processes, such as signal transduction, or receptor-mediated internalization. (Fraser et al., 1997; Girish & Kemparaju, 2007) HYA cells surface receptors include CD44, RHAMM (CD168), HARE, LYVE1, or TLRs with different functionalities. (Vigetti et al., 2014) For instance, the CD44 receptor is involved in various intracellular signaling pathways controlling hyaluronan internalization/degradation, angiogenesis, cell migration, proliferation, and aggregation. (Cyphert et al., 2015; Girish & Kemparaju, 2007; Knopf-Marques et al., 2016; Toole, 2004; Turley et al., 2002) The molecular weight of HYA is crucial for its activity: (i) Low-molecular-weight HYA (6–20 kDa) is linked with pro-inflammatory and angiogenesis gene expression processes, (ii) medium-molecular-weight HYA (20 kDa–1 MDa) plays role in embryogenesis, wound healing and regeneration and (iii) high-molecular-weight HYA (>1 MDa) is associated with anti-angiogenic and immunosuppressive effects. (Bayer, 2020; Sieger et al., 2019) Given its biological functions, HYA became one of the most widely used biopolymers in the biomedical sector, finding numerous applications in the fields of tissue engineering (soft tissue regeneration, wound treatment, 3D cell culture), ophthalmology, arthrology, urology, rhinology, pneumology, cosmetics, dietary, and drug delivery (cancer therapy). (Fallacara et al., 2018)

In the recent decade, HYA has also become of major interest to scientists focusing on its derivatization. In general, the main ideas behind the chemical modifications of HYA are to increase its application potential and/or to obtain high-performance products while maintaining at least some of the native HYA properties. There are essentially three general sites for synthetic modification: (i) the hydroxyl groups of GlcA unit, (ii) the carboxyl group of GlcA unit, and (iii) N-acetyl group of GlcNAc unit. These can be altered employing aqueous/non-aqueous syntheses or even reactions in solid-state (Larrañeta et al., 2018), which include simple “click chemistry” syntheses, the thiol-ene reaction, the Dies-Alder reactions, and azide-alkyne cycloaddition. (Felgueiras et al., 2017; Fu et al., 2017; Smith et al., 2018) The examples of HYA derivatives and their properties are summarized in several reviews. (Kim et al., 2019; Schanté et al., 2011) The applications of HYA derivatives are mostly focused on hydrogel formulations for tissue engineering and drug delivery systems. Besides the esterification, amidation, sulfation, and Ugi reactions, the selective oxidation of HYA can be carried out. Up to this date, there are three main oxidation routes employed for HYA: (i) 2,2,6,6-tetramethylpiperidin-1-yl)oxyl (TEMPO) (Ponedel’kina et al., 2015), (ii)

TEMPO/trichloroisocyanuric acid (TCC) (Shan et al., 2021), and (iii) $NaIO_4$ (periodate) oxidation (Pandit et al., 2019). The first two use TEMPO or TEMPO/TCC, which result in the oxidation of –OH at C6 of GlcNAc unit to –COOH or –CHO group, respectively. The periodate oxidation of HYA is regioselective towards vicinal –OH groups of GlcA which are oxidized to a pair of –CHO groups with simultaneous scission of the C2 and C3 bond, thus giving rise to 2,3-dialdehyde hyaluronate (DAH). Periodate oxidation of HYA was studied by *e.g.* Kristiansen et al., who focused on the macromolecular compaction of periodate oxidized hyaluronan. (Kristiansen et al., 2013) DAH is often utilized in biomedical sciences for hydrogel preparation, in which the highly reactive –CHO groups react with –OH groups (hemiacetalization) or $–NH_2$ groups (Schiff base formation) of the substrate. For example, DAH was used as a crosslinking agent in our recent comparative crosslinking study focused on the evaluation of the influence of various dialdehyde polysaccharides on poly(vinyl) alcohol-based hydrogel properties, (Muchová et al., 2022) for the preparation of hybrid chitosan hydrogels and their application in abdominal tissue regeneration, (Deng et al., 2017) or as a partially oxidized matrix crosslinked by adipic acid anhydride to form bio-printable hydrogel materials. (Weis et al., 2018)

The recent renaissance of periodate oxidation, historically used mainly in polysaccharide characterization, thus opens new synthetic routes for the preparation of many functional (bio)materials. However, one must keep in mind that the high reactivity of –CHO groups increases cytotoxicity of such derivatives as these groups can react with various targets of opportunity. Although still much less cytotoxic than low-molecular-weight crosslinkers such as glutaraldehyde, (Muchová et al., 2022) their cytotoxicity may not be suitable for various biomedical applications. Hence, in our recent study, (Münster, Fojtů, Capáková, et al., 2021) selected dialdehyde polysaccharide derivatives were further oxidized by chlorite to dicarboxylated derivatives, which showed reduced cytotoxicity profiles and improved characteristics. DAH was also transformed into 2,3-dicarboxylated hyaluronate (DCH, see Scheme 1 for reaction) for the first time and used as a drug delivery carrier for cisplatin (CP). However, the relatively harsh and un-optimized reaction conditions of sequential periodate-chlorite oxidation of HYA resulted in a dramatic decrease in molecular weight and only a partial degree of oxidation (*DO*) of the final DCH product. Nevertheless, this study showed extraordinary properties of DCH, namely its huge functionalization potential due to the essentially tripled number of –COOH groups per structural unit, low cytotoxicity in comparison with other dicarboxylated polysaccharides, high loading capacity and binding efficacy for CP, and increased cellular uptake in the case of MFC-7 breast cancer cell line with overexpressed CD44 receptors, which implied (at least partially) preserved affinity of DCH for these receptors.

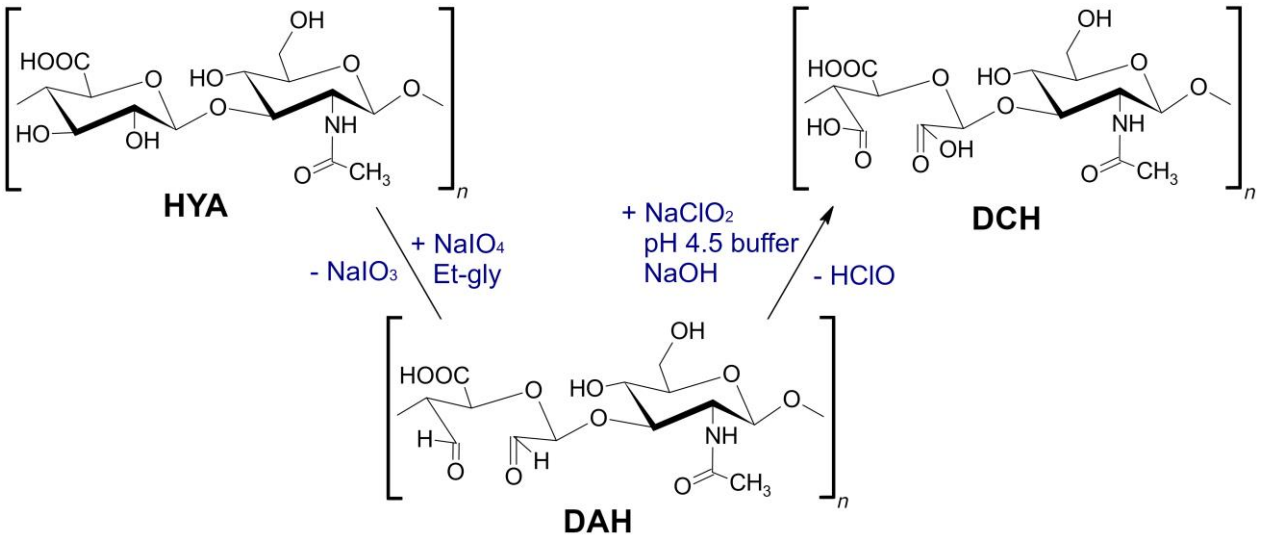

Scheme 1 Sequential periodate-chloride oxidation of hyaluronic acid.

Unlike the previous contributions focusing on the preparation, characterization, and utilization of periodate oxidized HYA, this work focus on the study of sequential periodate-chlorite oxidation of HYA to DCH for the first time. The influence of several DCH synthesis parameters (*i.e.* concentration of oxidizing agents, duration of oxidations, and molar ratio of reagents within periodate oxidation) on the physicochemical properties such as molecular weight distribution and *DO*, as well as cytotoxicity of resulting DCH derivatives, is studied. We hypothesize that the DCH properties (molecular weight, *DO*, *etc.*) can be modulated by the variation of periodate-chlorite oxidation conditions while maintaining a well-defined molecular structure. For this purpose, FT-IR, NMR spectroscopy, and DFT calculations were used to investigate the structural changes after sequential periodate-chlorite oxidation, while GPC and SEC-MALS-IV were employed for estimation of the molecular weight of prepared DCH materials. The conventional calibration method (GPC) was complemented by the multiple-detection method (SEC-MALS-IV) to investigate the influence of structural changes occurring upon hyaluronate oxidation on the resulting molecular weight estimation by GPC. Moreover, to exemplify the application potential of this material, cytotoxicity of selected DCH derivatives and HYA was established using NIH/3T3 cell line representing healthy cells and malignant epithelial ovarian cancer cell line A2780. The DCH and HYA were subsequently conjugated with various CP amount and their CP binding efficacy, CP content, and the release of CP were analyzed using XRF. The anticancer activity of the prepared conjugates against the A2780 cell line was evaluated and compared.

2. Materials and Methods

2.1 Materials

Sodium hyaluronate (HYA) (Contipro Ltd., Czech Republic) was used as a source polysaccharide for sequential periodate-chlorite oxidation. The weight-average molecular weight (M_w) was determined by

SEC-MALS-IV analysis to be 240 kDa (dispersity index D = 1.9, degree of polymerization calculated from weight-average molecular weight DP_w = 599). The second type of sodium hyaluronate (HYA2, M_w = 88.4 kDa, D = 1.52) from the same supplier was used only for the comparative cisplatin (CP) loading and release study. Sodium periodate ($NaIO_4$) and ethylene glycol (Penta, Czech Republic) were used in the primary oxidation of HYA. The resulting aldehyde groups of polysaccharide derivatives were subjected to secondary oxidation by sodium chlorite ($NaClO_2$, 80% RT) (Sigma Aldrich Co.) also employing glacial acetic acid (CH_3COOH) (Sigma Aldrich Co.), sodium acetate trihydrate ($CH_3COONa{\cdot}3H_2O$) (Penta, Czech Republic) and sodium hydroxide (NaOH) (Lachner, Czech Republic). The chemicals used in the characterization of the resulting hyaluronate derivatives included sodium chloride (NaCl) (Penta, Czech Republic), sodium nitrate ($NaNO_3$) (Lachner, Czech Republic), disodium phosphate dodecahydrate ($Na_2HPO_4{\cdot}12H_2O$) (VWR, Czech Republic), ethylenediaminetetraacetic acid (EDTA) and deuterium oxide (D_2O) (Sigma Aldrich Co.). For CP loading and release studies, silver nitrate ($AgNO_3$) (Sigma Aldrich Co.) and phosphate buffer saline (PBS) (Biosera, France) were used. Reagents used for the biological experiments included mycoplasma-free calf serum (CS) (Biosera, France), fetal bovine serum (FBS) (Biosera, France), penicillin-streptomycin (Biosera, France), trypsin-EDTA (Biosera, France), glutamine (Serva, Germany), Dulbecco's Modified Eagle's Medium (DMEM) (BioSera, France), RPMI-1640 (Biosera, France) and phosphate-buffered saline pH 7.2 (PBS) (Biosera, France), 3-(4,5-dimethylthiazol-2-yl)-2,5-diphenyl tetrazolium bromide (MTT) reagent (Duchefa Biochemie, Netherlands), dimethyl sulfoxide (DMSO) (Serva, Germany). All chemicals were of analytical grade and were used without further purification. Ultra-pure water (UPW) was used throughout the experiments.

2.2 Preparation of 2,3-dicarboxylated hyaluronates

Before primary periodate oxidation (POX), HYA was pre-dissolved (2 wt% solution) under vigorous stirring for 24 h at laboratory temperature. The POX started with the dropwise addition of concentrated $NaIO_4$ solution to the prepared HYA solution. The final concentration of HYA in POX solution was 1 wt%. The concentration of $NaIO_4$ in the reaction mixture of POX was set to 16.5 mg/mL (*i.e.* 77.1 mmol/L), and the molar ratio of HYA : $NaIO_4$ was 1:3.1. In the last series of experiments, the molar ratio of HYA : $NaIO_4$ was 1:1.25, *i.e.* 2.5× lower, while the $NaIO_4$ concentration was kept the same; the concentration of HYA in these experiments was increased accordingly due to lower volume. The influence of the reduced molar ratio of reactants on the properties (*e.g. DO*, M_w) of the final products was studied. The POX reaction mixtures were stirred at 30 °C in closed containers and in the absence of light for a given time (from 4 to 24 h). Subsequently, the oxidation reactions were terminated by the addition of excess ethylene glycol. The resulting 2,3-dialdehyde hyaluronate (DAH) samples were purified by dialysis employing dialysis tubing of 14 kDa molecular weight cut-off (*MWCO*) (Sigma Aldrich Co.) for 48 h. The purified products were filtered using 0.45 µm PVDF syringe filters, flash-frozen at -80 °C using an ethanol ice bath, and lyophilized.

Subsequently, DAH samples entered secondary oxidation (SOX) by $NaClO_2$ in the presence of pH 4.5 acetate buffer (0.045 M $CH_3COONa{\cdot}3H_2O$ and 0.055M acetic acid). The molar ratio of –CHO : $NaClO_2$ was set to 1:4, assuming 5.01 mmol/g of –CHO groups in DAH, *i.e.* the fully oxidized sample. (Münster, Fojtů, Capáková, et al., 2021) This fixed parameter was used to simplify the preparation of all DCH samples. The SOXs were performed in dark and started with the dropwise addition of concentrated $NaClO_2$ solution into the acidified solutions of DAH. Firstly, the influence of different $NaClO_2$ concentrations (0.05–0.5 M) in the

SOX reaction mixtures on the characteristics (IR and NMR spectra, M_w, *DO*) of final products was investigated. Secondly, the impact of the SOX reaction time from 4 to 24 h was investigated. The SOXs were terminated by the addition of 5 M NaOH to pH 8, products were purified by 48 h of dialysis using dialysis tubing of 14 kDa *MWCO*. After the dialysis, pH was set to 7.4 by diluted NaOH solution, samples were then filtered (0.45 μm), flash-frozen and lyophilized. The yields of all products of POX and SOX were calculated using known weights of source materials and resulting DAH or DCH products and molar masses of their structural units (M_{HYA} = 401 g/mol; M_{DAH} = 399 g/mol; M_{DCH} = from 453 to 475 g/mol depending on the *DO;* molar masses of DCH structural units were calculated as a weighted average of oxidized and non-oxidized units based on known *DO*). The yields of all products were almost quantitative (above 95%, see Table S2). The resulting 2,3-dicarboxylated hyaluronates (DCH) in the form of sodium salts were designated according to the parameters of POX and SOX (Table 1). A total of four series of DCH samples were prepared based on: (i) the concentration of $NaClO_2$ in SOX (Series A), (ii) the duration of SOX (Series B), (iii) the duration of POX (Series C) and (iv) the duration of POX while employing a reduced molar ratio of HYA : $NaIO_4$ (Series D). Note that three of the synthesized DCH samples (A-DCH-02, B-DCH-04, and C-DCH-04) were prepared using equal reaction conditions. This crosspoint among the three different series served for the evaluation of the reproducibility of DCH synthesis. All prepared DCH samples were analyzed by the methods described below and selected DCH samples were loaded with CP.

Table 1 Designation of the prepared DCH samples reflecting the studied parameters of POX (t_{POX} – duration and n_{HYA} : n_{NaIO4} – molar ratio of polysaccharide to periodate) and SOX (t_{SOX} – duration and c_{NaClO2} – concentration of chlorite) highlighted in bold.

		POX		SOX	
	Sample	**t_{POX} (h)**	**n_{HYA} : n_{NaIO4} (mol : mol)**	**t_{SOX} (h)**	**c_{NaClO2} (mol/L)**
Series A	A-DCH-01	24	1:3.1	24	***0.05***
	A-DCH-02	24	1:3.1	24	***0.1***
	A-DCH-03	24	1:3.1	24	***0.2***
	A-DCH-04	24	1:3.1	24	***0.3***
	A-DCH-05	24	1:3.1	24	***0.5***
Series B	B-DCH-01	24	1:3.1	***4***	0.1
	B-DCH-02	24	1:3.1	***8***	0.1
	B-DCH-03	24	1:3.1	***12***	0.1
	B-DCH-04	24	1:3.1	***24***	0.1
Series C	C-DCH-01	***4***	1:3.1	24	0.1
	C-DCH-02	***8***	1:3.1	24	0.1
	C-DCH-03	***12***	1:3.1	24	0.1
	C-DCH-04	***24***	1:3.1	24	0.1
Series D	D-DCH-01	4	***1:1.25***	24	0.1
	D-DCH-02	8	***1:1.25***	24	0.1
	D-DCH-03	12	***1:1.25***	24	0.1
	D-DCH-04	24	***1:1.25***	24	0.1

2.3 FT-IR, DFT, NMR structural analyses

Qualitative FT-IR analysis was carried out on the source material and all of the prepared hyaluronate derivatives and selected CP conjugates using an infrared spectrometer Nicolet 6700 FT-IR (Thermo Fisher Scientific, USA) equipped with the diamond crystal using ATR mode in a span of wavelengths 4000–500 cm^{-1} (res.: 4, scans: 64, the suppression of atmospheric gases enabled).

Structures of HYA, DCH, and respective CP-conjugates were optimized at the DFT level of theory employing a PBE0 functional and the standard def-SVP basis sets. (Adamo & Barone, 1999; Weigend & Ahlrichs, 2005) The PCM solvent model was used to simulate the aqueous environment and Grimme's D3 dispersion correction was included for a better description of weak interactions. (Grimme, 2006) Subsequently, CP residues were bound to suitable –COOH groups of optimized structures and conjugates re-optimized using PBE0 functional and def2-TZVPP basis set with ECP replacing 60 core electrons for platinum and def2-SVP basis set for lighter atoms. (Andrae et al., 1990, 1990) This setup was previously calibrated for the calculation of structures of platinum complexes. (Münster, Fojtů, Capáková, et al., 2021; Pawlak et al., 2014)

The ^{1}H, ^{13}C, and $^{1}H–^{13}C$ correlation spectra were obtained for 10 mg/mL samples using a Bruker Avance III HD 700 MHz NMR spectrometer (Bruker, USA) equipped with a triple-resonance cryoprobe optimized for ^{13}C detection at 298 K in D_2O. ^{1}H spectra used for signal quantification were recorded using a 30° excitation pulse, the acquisition time of 5 s, the delay between pulses of 5 s, and 128 scans. This setup was previously found to provide good quantitative results for other selectively oxidized polysaccharides. (Münster et al., 2020) The $^{1}H–^{13}C$ multiplicity-edited heteronuclear single quantum correlation (HSQC, $J_{H–C}$ = 145 Hz) and $^{1}H–^{13}C$ heteronuclear multiple bond correlation (HMBC, ${}^{n}J_{H–C}$ = 10 Hz) experiments were used based on the previous experiences. (Münster et al., 2017; Münster, Fojtů, Capáková, et al., 2021) The *DO* of the prepared DCH samples, *i.e.* the percentage of basic structural units of HYA converted to 2,3-dicarboxylated hyaluronate units, (Münster, Fojtů, Capáková, et al., 2021) was determined from NMR spectra by the comparison of H4 and H5 signal intensities of the of oxidized units (4.0–4.2 ppm) and well-separated H1 signal of unoxidized HYA (4.38 ppm). Because HYA units are converted to oxidized DCH units, the sum of their signal intensities corresponds to 100% of the total signal, and the *DO* (%) = 1 - [Int_{HYA}/(Int_{HYA} + Int_{DCH})] × 100, where Int_{HYA} is the intensity of H1 signal (HYA) and Int_{DCH} an average of H4 and H5 signal intensities.

2.4 GPC and SEC-MALS-IV macromolecular analyses

Initially, DCH samples' molecular weight distribution was analyzed by the gel permeation chromatography (GPC), a type of size-exclusion chromatography employing conventional calibration, using a Waters HPLC Breeze chromatographic system set up with a Tosoh TSK gel $GMPW_{XL}$ column (300 mm × 7.8 mm × 13 µm, column T = 30 °C) (Tosoh, Japan) and a Waters 2414 refractive index detector (drift tube T = 60 °C) (Waters, USA). A mixture of 0.1 M $NaNO_3$ and 0.05 M $Na_2HPO_4 \cdot 12H_2O$ was employed as a mobile phase. Calibration was carried out using pullulan polysaccharide calibration kit SAC-10 (Agilent Technologies, USA) in a span of M_w 342–805000 g/mol.

To obtain an absolute characterization of molecular weight distribution, size exclusion chromatography coupled with multi-angle light scattering, and intrinsic viscosity (SEC-MALS-IV) analysis were used employing HPLC Infinity II system (Agilent Technologies, USA) set up with a Shodex LB-806M column (300

mm × 8.0 mm × 13 µm), Shodex RI-501 refractive index detector (T = 25 °C) (Shodex, Japan), Wyatt DAWN Heleos II multi-angle light scattering and ViscoStar III viscosity detectors (Wyatt Technology, USA). 0.15 M $NaNO_3$ containing 10 mM EDTA mobile phase and specific index increment dn/dc = 0.150 mL/g were used.

2.5 In vitro cytotoxicity study

Selected DCH samples, their CP-conjugates, one DAH sample (t_{POX} = 24 h, n_{HYA} : n_{NaIO4} = 1:3.1), and source sodium hyaluronate along with its CP-conjugate were evaluated in the terms of their cytotoxicity against an immortalized mouse embryonic fibroblasts cell line NIH/3T3 (ECACC 93061524, UK), which represents healthy cell line. Next, the cytotoxicity of the two most promising DCH samples and HYA2, CP-DCH conjugates, and CP-HYA2 conjugate was investigated against malignant epithelial ovarian cell line A2780 (ECACC 93112519, UK). DMEM containing 10% of CS and RPMI-1640 containing 10% of FBS and 2 mM glutamine was used as a cell-culture media for NIH/3T3 and A2780, respectively. Both media were supplemented by 100 U/mL of penicillin, and 0.1 mg/mL of streptomycin. The cells were cultivated using an incubator tempered at 37 °C and humidified mixture of ambient air and 5% CO_2. Subsequently, cells were seeded onto a 96-well plate at a density ensuring 70% confluence on the day of treatment. The treatment was performed on the second day of cultivation when the culture medium was replaced with a fresh one containing hyaluronate/derivatives (100 µL per well, concentration range 0–20 mg/mL and 0–100 µM for hyaluronate/derivatives and CP-conjugates, respectively). After another 48 h, the cell-culture medium containing hyaluronate derivatives was removed and the cells were incubated with a fresh medium containing 1 mg/mL of MTT reagent for another 4 h. Plates with the cells were wrapped in aluminium foil and kept in a humidified atmosphere at 37 °C. Next, the MTT culture medium was replaced by DMSO to dissolve the formazan crystals; the well plate was gently shaken and the absorbance at 570 nm was recorded using a microplate reader Infinite 200PRO (Tecan, Switzerland). The IC_{50} values were then calculated by fitting the data with the logistic function to create a sigmoidal dose-response curve. All measurements were performed in quadruplicates.

2.6 CP-conjugates preparation, loading, and release study

CP was prepared as described in the literature. (Wilson & Lippard, 2014) It was chosen as a model drug because of its wide adoption in clinical practice. For conjugation, the synthesized CP solutions (0.66 mg/mL, 2mg/mL, and 3.33 mg/mL) were activated using $AgNO_3$ (molar ratio 1:2.1) for 16 h at 55 °C and the formed AgCl precipitate was filtered out (0.22 µm PTFE syringe filters). Next, a few drops of 1 M NaCl solution were added to activated CP solutions to remove the residual Ag^+ ions, the mixtures were cooled and filtered again. This procedure ensures the complete elimination of chlorido ligands from the CP and the formation of reactive $[(NH_3)_2Pt(H_2O)_2](NO_3)_2$ complex, which readily reacts with –COOH groups of the DCH and HYA. The concentration of the activated CP was determined by quantitative elemental analysis carried out utilizing an energy-dispersive X-ray fluorescence (XRF) spectrometer ARL Quant'X EDXRF Analyzer (Thermo Scientific, USA). The calibration standards were prepared by dissolving a specific amount of CP in water.

Activated CP solutions were then mixed with 5 mg/mL solutions of C-DCH-01, C-DCH-04, and sodium hyaluronate (HYA2, see Section *2.1*) resulting in the loading ratios of CP : carrier = 2:10, 6:10, and 10:10 (w/w). These reaction mixtures were then gently shaken for 96 h at laboratory temperature in the dark,

following our earlier works. (Münster et al., 2019) The solutions containing CP-conjugates were subsequently dialyzed for 3 h using 3.5 kDa *MWCO* dialysis tubing (Thermo Scientific, USA) against water to remove unbound CP, flash-frozen, and lyophilized. CP-loaded samples were designated as CP-DCH-01, CP-DCH-04, and CP-HYA2. CP loading efficacy was subsequently analyzed by XRF.

The CP release kinetics of selected CP-conjugates (CP-DCH-01, CP-DCH-04, and CP-HYA2 loaded using 6:10 CP : carrier w/w ratio) were investigated and compared using a previously employed setup that simulates *in vitro* conditions. (Münster et al., 2019) Briefly, 10 mg of each CP-conjugate was mixed with 5 mL of 7.4 pH PBS, sonicated by employing an ultrasonic homogenizer Sonopuls HD2070 (Bandelin, Germany) equipped with MS 73 microtip. Homogenized CP-conjugates were then transferred into 3.5 kDa *MWCO* dialysis tubing and placed in 95 mL of 7.4 pH PBS release media heated to 37 °C. Aliquot samples (5 mL) were collected over 48 h and replaced each time with 5 mL of fresh 7.4 pH PBS to conserve the volume. To simplify the discussion, the term CP is in the following text used also for released cisplatin residuum, *i.e.* the cis-$[Pt(NH_3)_2(H_2O)_2]^{2+}$ complex. The quantitative elemental analysis of CP-conjugates and aliquot samples of released CP was carried out using XRF.

3. Results and discussion

First of all, the design of the experiments within this study needs to be addressed. Instead of starting with an investigation of POX conditions (t_{POX} – reaction duration, n_{HYA} : n_{NaIO4} – HYA and periodate oxidizing agent molar ratio) as one may expect, it was decided to first evaluate the importance of the concentration of $NaClO_2$ within SOX (c_{NaClO2}), which was previously found to be a crucial parameter significantly affecting both the distribution of molecular weight momentums and the molecular composition of various oxidized polysaccharides. (Münster et al., 2020) Thus, in the first set of experiments (Series A, see Table 1), the values of POX parameters (t_{POX} = 24 h, n_{HYA} : n_{NaIO4} = 1:3.1), as well as the duration of SOX (t_{SOX} = 24 h), were fixed based on previous research. (Münster, Fojtů, Capáková, et al., 2021) The only remaining variable, the c_{NaClO2} in SOX, was systematically varied from 0.05 to 0.5 M to determine the optimal $NaClO_2$ concentration, which would still ensure complete oxidation while minimizing the degradation effects induced by SOX. On the one side, the very low molar concentrations of the oxidizing agent should not drastically influence (decrease) the molecular weight of resulting DCH but they may not be sufficient to fully oxidize –CHO groups even after 24 h SOX. On the other hand, the use of higher $NaClO_2$ concentrations (0.5 M) leads to fast oxidation, (Münster, Fojtů, Capáková, et al., 2021), but could also induce DCH degradation later on. The second set of experiments (Series B) was focused on the influence of the duration of SOX on the properties of the final material. Shortening of SOX reaction time may have positive (*e.g.* reduced degradation) but also negative (insufficient oxidation) influence on the properties of the resulting materials and possibly render the whole process more effective. The conditions of POX remained fixed and the optimal concentration of $NaClO_2$ in SOX established in the Series A was employed. Combined, Series A and B allow to optimize the SOX parameters. Next, these parameters (c_{NaClO2} and t_{SOX}) were fixed and the influence of POX duration (t_{POX}) on the DCH properties was investigated in the span from 4 to 24 h using 1:3.1 molar ratio of HYA : $NaIO_4$ (Series C) and 1:1.25 molar ratio (Series D). The variation of t_{POX} parameter should affect mostly the *DO* and molecular weight of the product, while the decrease molar ratio may still be sufficient to completely oxidize HYA while suppressing degradation of macromolecules.

3.1 FT-IR and NMR structural study

To obtain detailed information about DCH structures, the prepared DCH samples were investigated using a combination of ^{1}H, ^{13}C, and $^{1}H–^{13}C$ HSQC and $^{1}H–^{13}C$ HMBC NMR spectra and FT-IR spectroscopy. The ^{1}H NMR spectra of all DCH samples within the respective series and the ^{1}H and ^{13}C, HSQC, and HMBC NMR spectra of the fully oxidized C-DCH-04 sample can be found in Figures S1–S5 in Supporting Information (SI). To describe the changes occurring during the sequential oxidation, ^{1}H spectra of selected DCH samples (C-DCH-01 and C-DCH-04) and source HYA were analyzed first (Figure 1). The oxidation of HYA can be observed for instance by the disappearance of the H1 and CH_3 group signals at 4.38 ppm and 1.95 ppm, respectively. The ^{1}H spectra of the fully oxidized DCH sample then contain 11 major signals, three of which were assigned to protons at C1 (4.66 ppm), C4 (4.08 ppm), and C5 (4.21 ppm) of the GlcA group based on the $^{1}H–^{13}C$ correlation spectra (Figure S5c), while the remaining eight signals belong to intact GlcNAc units resistant to the periodate oxidation due to the presence of β-(1→3) glycosidic bonds and the N-acetyl group at C2'. The full ^{1}H and ^{13}C signal assignment of DCH is given in Table S1 in SI. The NMR spectra confirm the oxidation of the GlcA units in 2,3-dicarboxylated derivatives and the presence of intact GlcNAc units.

Note that while the signals of unoxidized HYA are still apparent in the C-DCH-01 spectrum in Figure 1, see *e.g.* signal of H1 at 4.36 ppm, only their residues remain in the spectrum of the C-DCH-04 sample. The NMR spectra were thus used to determine the *DO*s of individual samples, defined as the percentage of basic structural units of HYA converted to 2,3-dicarboxylated hyaluronate units, and these are given in Figure 3.

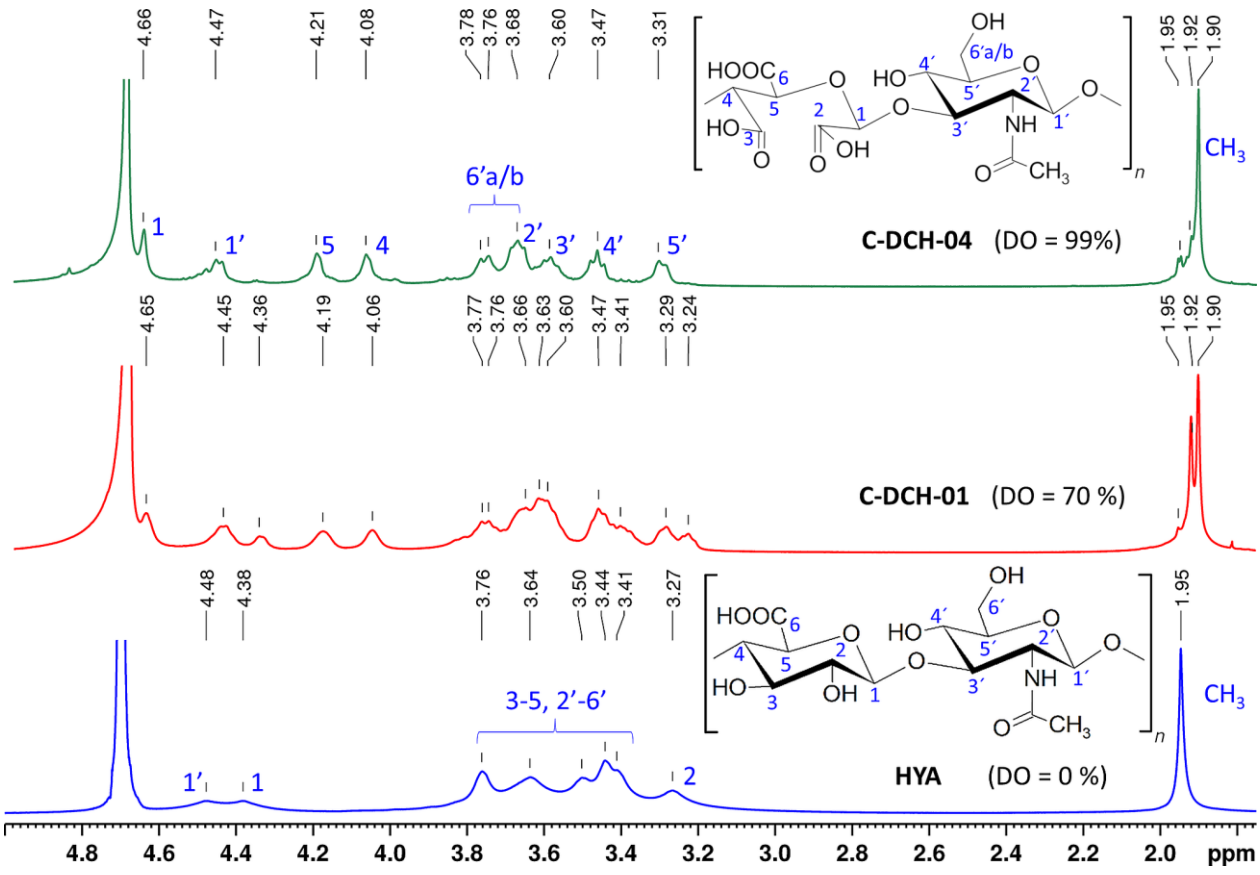

Figure 1 ^{1}H NMR spectra of source HYA, C-DCH-01, and C-DCH-04 samples measured at 298 K in D_2O.

The IR spectra of DCH samples prepared within Series A and source HYA are given in Figure 2, while the spectra of selected DCH samples from other series are given in SI, Figure S6. Findings from FT-IR analysis complement the NMR study. Generally, the HYA (bottom spectrum of Figure 2) exhibits several characteristic IR vibrational bands located at around 1600 cm^{-1} (asymmetric valence $–COO^-$ vibration), 1425 cm^{-1} (symmetric valence $–COO^-$ vibration), 1380 cm^{-1} (–OH deformation, –COOH monomer form), 1035 cm^{-1} (symmetric valence –C–O–C– vibration) and 893 cm^{-1} (C–H deformation of the GlcA unit). The last-mentioned vibration is considered as a GlcA unit fingerprint and thus can be used to evaluate (at least on the qualitative level) the presence of unoxidized GlcA units of hyaluronate. The sequential oxidation leads to the disappearance of this band thus signifying extensive, most likely complete HYA oxidation accompanied by scission of C2 and C3 bond of HYA's GlcA units. Furthermore, the HYA sequential oxidation also leads to the steep increase of absorption band intensity at 1600 cm^{-1} and the appearance of new vibrational bands at 1320 cm^{-1} (–COOH valence vibration of dimer form) and 850 cm^{-1} (–CH deformation, –CHO group) corresponding to the formation of new –COOH groups at C2 and C3.

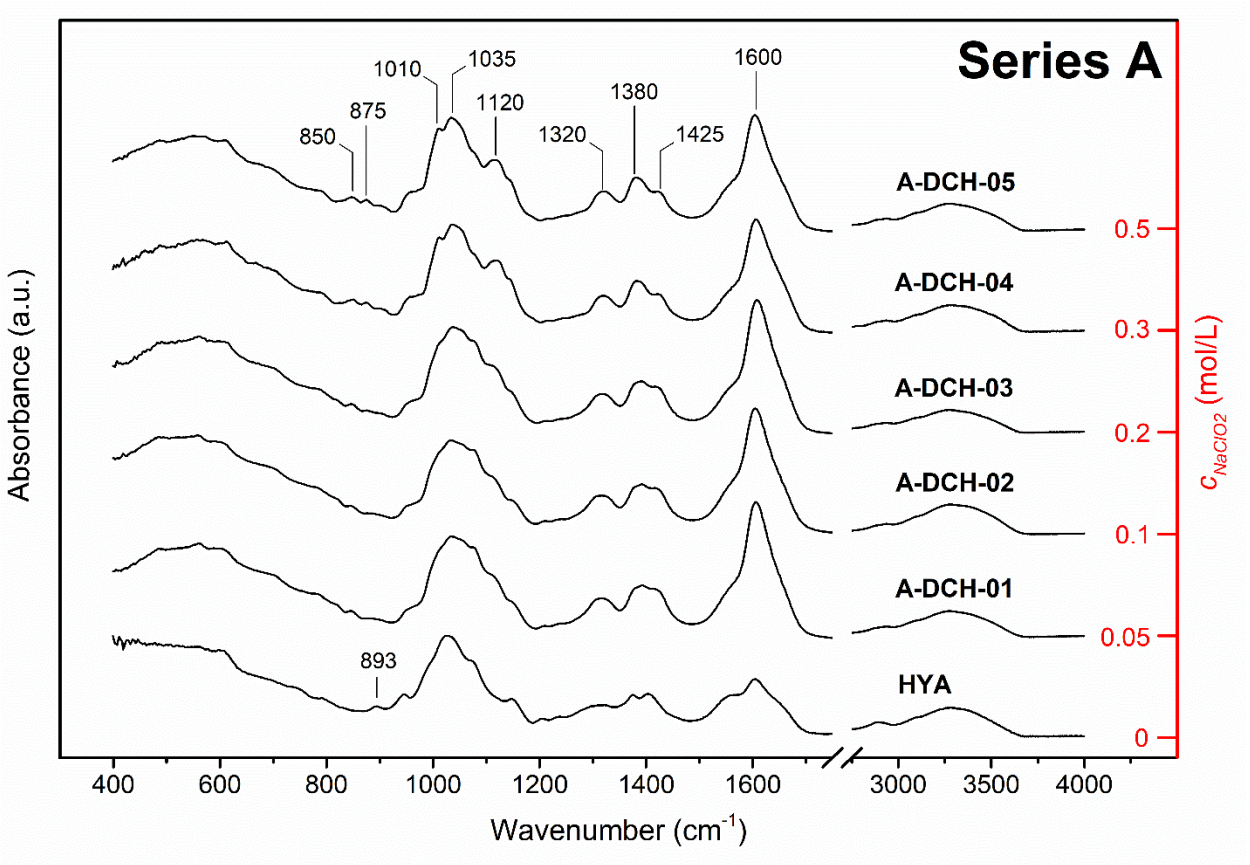

Figure 2 FT-IR analysis of the DCH samples prepared within Series A (variable c_{NaClO2} in SOX).

Regarding individual series, the IR spectral analysis of the A-DCH samples (Figure 2) showed the appearance of similar spectral patterns across the entire Series A regardless of the $NaClO_2$ concentration. Nevertheless, slight changes in IR spectra of A-DCH samples can be found with increasing $NaClO_2$ concentration. The first distinguishable change is the significant increase in the signal intensities of vibrational bands at 1120 cm^{-1}, 1010 cm^{-1} (both symmetric valence –C–O–C–), 1380 cm^{-1}, and the appearance of a new band at 875 cm^{-1}. These changes are best visible in the spectra of A-DCH-04 and A-DCH-05 (*i.e.* those oxidized using the two highest $NaClO_2$ concentrations, 0.3 and 0.5 M, respectively) but can be also seen in the spectra of A-DCH-03 (0.2 M $NaClO_2$), although not at the same magnitude. The appearance of these signals can be attributed to non-selective oxidation of GlcNAc unit induced by the relatively high concentration of $NaClO_2$ (or by hypochlorite formed in the reaction mixture) which presumably attacks –OH groups located on C6' of GlcNAc unit forming an additional carboxyl or carbonyl groups, whose presence influences the vibrations of nearby hemiacetal (–C–O–C–) group. This assumption is further supported by a gradual broadening of the 1600 cm^{-1} band with increasing $NaClO_2$ concentration, indicating a formation of another kind of –COOH groups (presumably at C6') with different chemical surroundings than the existing ones, which influences these –COOH asymmetric valence vibrations.

The ^1H NMR spectra of A-DCH samples are given in Figure S1. As the molar concentration of $NaClO_2$ increases, the signal of H5' and H6' protons disappears (c_{NaClO2} > 0.2 mol/L) while new signals appear between 4.2–4.9 ppm. These changes are consistent with undesirable oxidation at C6' by a high concentration of $NaClO_2$ indicated by IR spectra. Hence, the 0.1 M $NaClO_2$ concentration, which allows full oxidation of HYA without any observable adverse effects, was selected for further studies.

The duration of SOX (from 4 to 24 h) was investigated in Series B with c_{NaClO2} set to 0.1 mol/L. The two examples of IR spectra of B-DCH samples prepared by the shortest and the longest SOX reaction times (B-DCH-01 – 4 h SOX, B-DCH-04 – 24 h SOX) can be found in Figure S6 (left part) in SI. Briefly, these spectra show two major differences: (i) the B-DCH-01 exhibits stronger signal intensity at 1110 and 875 cm^{-1} bands (symmetric valence –C–O–C– vibration and –CH deformation of –CHO groups, respectively) signifying the presence of residual unoxidized aldehyde groups originating from POX presumably forming hemiacetals. These bands are not present in the B-DCH-04 sample where all aldehyde/hemiacetal groups were highly oxidized throughout 24 h reaction. (ii) The intensity of the band at 1600 cm^{-1} is comparably stronger in B-DCH-04 than in B-DCH-01 which evidences the higher number of –COOH groups formed at C2 and C3. The ^1H NMR spectra of Series B samples are given in Figure S2. The signals of unoxidized GlcA units of HYA are absent in all spectra, indicating high overall *DO* after POX. However, the spectra of samples prepared using short SOX contain several additional signals, *e.g.* around 1.95, 3.90, and 4.90 ppm. These signals were assigned to hemiacetals between the –CHO groups at C2 or C3 and available –OH groups in the DCH chain, which withstood the conditions of shorter SOX. Their intensity decreases from ~60% of the intensity of H4 and H5 signals (B-DCH-01 sample, 4 h SOX) to a few percent (B-DCH-04 sample, 24 h SOX). Longer SOX times are thus required to convert residual hemiacetals to carboxylates, which is in agreement with IR spectra. The duration of SOX was thus fixed to 24 h to minimize the number of prevailing hemiacetals.

The last two sets of experiments were focused on the variation of POX duration (t_{POX}) under two different molar ratios of HYA : $NaIO_4$ (1:3.1 – Series C, 1:1.25 – Series D) while maintaining previously optimized SOX

parameters (c_{NaClO2} = 0.1 M; t_{SOX} = 24 h). The IR spectra of the C and D series prepared using the shortest and the longest POX are depicted in Figure S6 (middle and right part). Both series showed similarities in the spectral patterns, *i.e.* the IR spectra of samples oxidized for 4 h (C-DCH-01 and D-DCH-01) exhibit bands at 1150 cm^{-1} (R–OH deformation) and 893 cm^{-1} (C–H deformation, GlcA unit fingerprint) of similar intensity implying the presence of intact unoxidized glucuronate units of HYA, see cutouts in the middle and right part of Figure S6. In the case of t_{POX} = 24 h, the band at 893 cm^{-1} is barely visible in the IR spectrum of C-DCH-04, while a recognizable peak is present in the D-DCH-04 spectrum. The NMR spectra of the C (Figure S3) and the D (Figure S4) series confirm the findings from the FT-IR analysis. The stronger residual signals of H1 from HYA in the spectra of D-series samples indicate the lower *DO* compared to Series C as a consequence of a 2.5× lower molar ratio of HYA to $NaIO_4$ used in sample preparation. The largest differences in *DO* (82 *vs.* 95%) were found in samples prepared using t_{POX} = 12 h (Figure 3).

Altogether, the utilization of c_{NaClO2} = 0.1 M and t_{SOX} = 24 h, in conjunction with a higher molar ratio of HYA : $NaIO_4$ and t_{POX} = 24 h results in the preparation of highly oxidized DCH material without non-selective oxidation or under oxidation. Partially oxidized DCH can be obtained by simply decreasing the duration of POX, while the conditions of SOX should be preserved to minimize the number of residual hemiacetals.

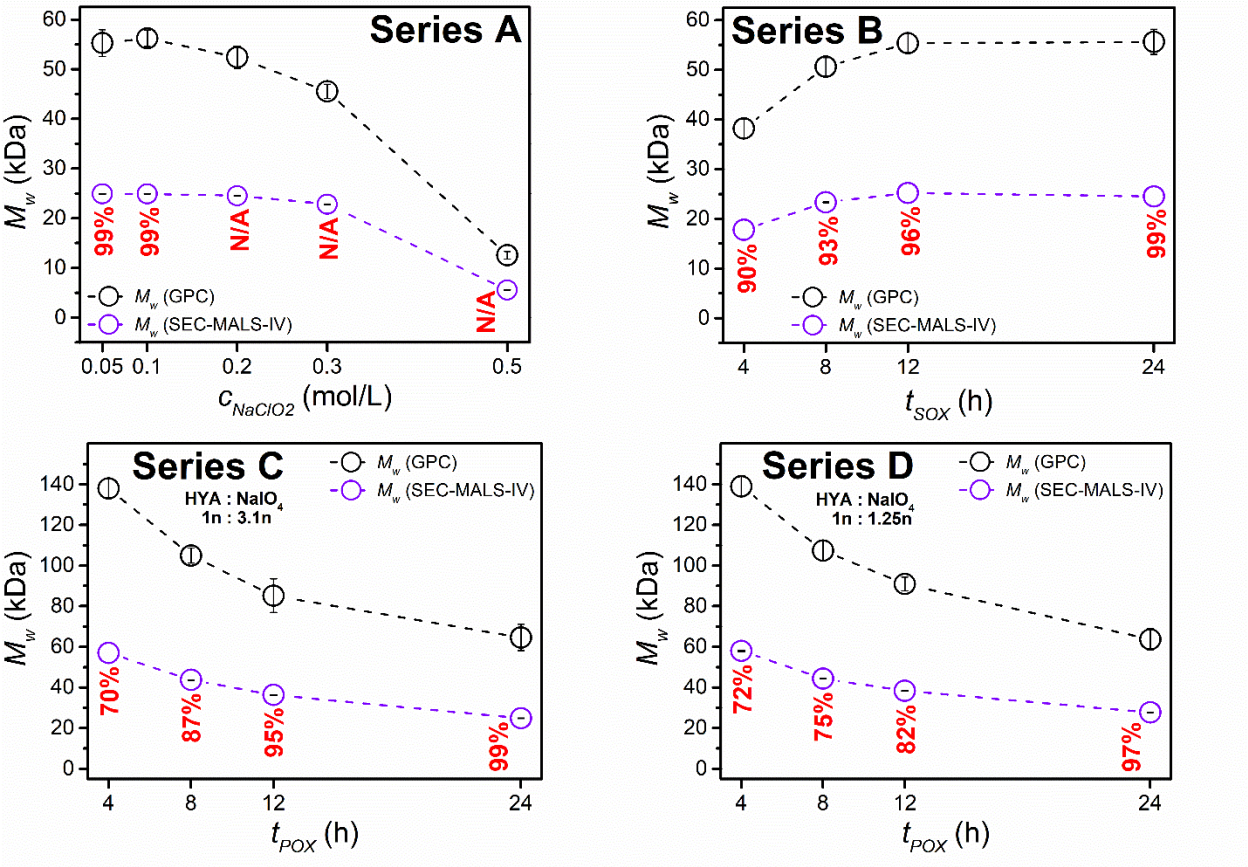

Figure 3 The dependence of DCH weight-average molecular weight (M_w) estimated by GPC (black line) and SEC-MALS-IV (violet line) on the: (A) concentration of $NaClO_2$ in SOX, (B) duration of SOX, (C) duration of

POX employing high HYA : $NaIO_4$ molar ratio and (D) duration of POX employing low HYA : $NaIO_4$ molar ratio. The error bars represent the standard deviation. The degrees of oxidation (*DO*) of all prepared DCH samples obtained in the NMR study are noted in red and express the ratio of unoxidized HYA units to fully-oxidized DCH units containing two –COOH groups per unit. The dashed lines connecting data points are only guides for the eyes.

3.2 Molecular weight analysis

To investigate the dependence of the varied synthesis parameters on the DCH molecular weight distribution, all prepared DCH samples were analyzed using GPC with pullulan standards and SEC-MALS-IV (see Section *2.4*). The M_w plots for each series are given in Figure 3 and the detailed results are summarized in the SI (Table S2). Furthermore, Mark-Houwink-Sakurada (MHS) plots are given in Figure S7.

First, we address the differences between GPC and SEC-MALS-IV techniques. Both the GPC and SEC-MALS-IV measurements are based on the separation of the analyte macromolecules of different hydrodynamic volumes in the stationary porous gel phase and subsequent faster elution of larger over smaller macromolecules, *i.e.* both are based on size-exclusion chromatography. In the case of GPC analysis, however, the molecular weight of an unknown sample is estimated based on conventional calibration using selected calibration standards. On the other hand, the SEC-MALS-IV technique enables the determination of molecular weight momentums absolutely via multiple detections, and thus independently of calibration standards. By comparison of these techniques, we seek to point out the limitations of GPC, which is broadly used in the molecular weight characterization of various polymers and their derivatives while using a common set of standards. This leads to disregarding structural differences between the standard and the analyte. We also seek to elucidate how highly charged/partially oxidized DCH affects GPC measurements. The black ($M_{w\,GPC}$) and purple ($M_{w\,SEC\text{-}MALS\text{-}IV}$) lines in Figure 3 exemplify the discrepancy in the data obtained by the used techniques.

The increase of c_{NaClO2} within A Series was accompanied by a progressive decline of M_w of respective A-DCH samples. The low c_{NaClO2} (A-DCH-01 – 0.05 M and A-DCH-02 – 0.1 M) gave rise to the products of M_w 55 kDa (D = 2.1) according to GPC, but only 25 kDa (D = 1.6) according to SEC-MALS-IV, *i.e.* more than 2× lower value than the GPC estimate. As the c_{NaClO2} grew larger, M_w of resulting DCH decreased relatively to A-DCH-02 by about 1.6% for A-DCH-03, 8.5% for A-DCH-04, and a staggering 77.5% for A-DCH-05 sample as measured by SEC-MALS-IV. These observations go well in line with the results obtained in FT-IR and NMR study – the harsher the oxidation conditions are, the more the structural defects and the lower molecular weight products are obtained. It should be emphasized, that analogous trends were observed by both SEC-MALS-IV and GPC, although at a different scale. This exact phenomenon of data proportionality was observed also in other series, albeit of variable magnitude.

Next, the prolongation of SOX (t_{SOX} = 4–24 h) led to a steady rise of DCH M_w in the B series (see Figure 3). Essentially, as a part of –CHO groups is left unoxidized during shorter SOX, partially oxidized DCH materials containing a mixture of –CHO and –COOH groups are obtained. Concomitantly, the prolongation of SOX results in a higher conversion of –CHO to –COOH/–COO^-Na^+ groups, which increases the molecular weight of DCH samples (M_w increased with t_{SOX} from 17.8 to 24.5 kDa and from 38 to 56 kDa according to SEC-MALS-IV and GPC, respectively). Such behavior was previously observed by us also for sequential oxidation

of cellulose. (Münster et al., 2020) Moreover, as the *DO* increases from 90 to 99%, the $M_{w\ GPC}/M_{w\ SEC\text{-}MALS\text{-}IV}$ ratio increases from 2.15 to 2.27 which indicates that GPC measurements are further affected by: (i) the presence of residual hemiacetal bonds and –CHO groups in samples with smaller *DO*, which is presumably resulting in more compact "crosslinked" macromolecular coils and (ii) increased electrostatic repulsion of –COOH groups in samples of high *DO,* resulting in an increased hydrodynamic volume.

Last, the influence of POX duration (t_{POX} = 4–24 h) and POX reactant molar ratio (n_{HYA} *:* n_{NaIO4} = 1:3.1 and 1:1.25) on the molecular weight distribution of C and D series samples were investigated (see Figure 3). In both cases, the M_w of DCH is decreasing with the increasing duration of the POX. The differences between the molecular weight distribution within C and D Series are relatively small (≤11.6% and ≤6.4% according to SEC-MALS-IV and GPC, respectively). In other words, the shortening of POX reaction times (4–8 h) leads to higher-molecular-weight DCH products (M_w = 57–44 kDa according to SEC-MALS-IV and of 138–107 kDa according to GPC), although at the cost of partial oxidation (*DO* = 70–87%) as confirmed by FT-IR and NMR study (see Section *3.1*). The polysaccharide : periodate molar ratio is thus of relatively minor importance towards M_w, but it significantly influences *DO.*

Generally, the sequential oxidation of HYA resulted in a considerable decrease in M_w of all prepared DCH samples compared to the source material, although degradation did not reach the extent reported previously (DCH product of 94% reduction of M_w according to GPC at 70% *DO*). (Münster, Fojtů, Capáková, et al., 2021) Note, that extensive periodate oxidation of HYA (up to *DO* = 80%) has been previously shown to cause no significant decrease in M_w, (Kristiansen et al., 2013) in contrast to alginates (Vold et al., 2006), and chitosans (Vold & Christensen, 2005). It should be noted, however, that study of Kristiansen et al. focused primarily on periodate-oxidized HYA which was subsequently reduced by borohydride, converting free –CHO groups to hydroxyls. The question stands whether this reduction was sufficient to fully disrupt also the hemiacetal network formed during the oxidation, particularly given the known stability of intermolecular hemiacetals in various polysaccharides. (Maia et al., 2011; Münster et al., 2020) If not, remaining intermolecular hemiacetals could affect the molecular weight of resulting reduced DAH. Nevertheless, the chlorite oxidation of DAH is undeniably a crucial step influencing the molecular weight of resulting DCH as expected. To summarize, after POX and SOX optimization, the largest fully oxidized (99% *DO*) DCH sample exhibits roughly 74% (55 kDa) decrease in M_w according to GPC. Note, however, that this corresponds to a 90% (25 kDa) decrease according to SEC-MALS-IV with the respect to source HYA. The largest partially oxidized (72% *DO*) DCH sample exhibits a 42% (139 kDa) and a 75% (58 kDa) decrease according to GPC and SEC-MALS-IV relatively to source HYA, respectively. The prepared derivatives can be recognized as medium molecular weight HYA derivatives with a DP_w between 50 to 130.

The exact mechanism of DCH degradation is not clear. However, the observed decrease of molecular weight of prepared DCH samples was progressing with increasing *DO, i.e.* when more of the C2-C3 bonds are broken. This implies the possible crucial role of the GlcA C1–O–C5 hemiacetal bond, which could be disrupted by an acidic and aggressive oxidizing environment during the secondary oxidation. Besides, the possible evolution of hypochlorite during secondary oxidation may lead to random non-selective oxidation reactions causing scission of other glycosidic bonds. (Sirviö et al., 2014)

Regarding the differences between GPC and SEC-MALS techniques, the main limitation of GPC arises from the choice of standard. In this case, pullulan was selected as a standard for GPC column calibration as it

beneficially shares both the linear character and polysaccharide origin with the HYA. However, the DCH macromolecules are composed of periodate-opened GlcA units, which significantly increases their flexibility. (Kristiansen et al., 2010) Furthermore, a large density of –COOH groups causes a strong electrostatic repulsion of these flexible chains and the formation of large ionic corona around the coil; the relatively small DCH macromolecule thus may occupy a relatively large hydrodynamic volume, which has a crucial impact on the results of GPC measurements, causing an overestimation of molecular weights by a factor of 2.3 ± 0.1 compared to SEC-MALS. It should be also noted, that the overestimation of molecular weight values of hyaluronate samples obtained by GPC measurements (using pullulan standards for conventional calibration) was previously investigated and attributed to the nature of calibration standards and sample concentration. (Shanmuga Doss et al., 2017) The overestimation of molecular weights by GPC measurements would thus likely apply also to other dicarboxylated polysaccharides, such as those studied earlier by us. (Münster et al., 2020; Münster, Fojtů, Capáková, et al., 2021; Münster, Fojtů, Muchová, et al., 2021) Nevertheless, it was shown that GPC can still be employed to estimate relative results on molecular weight as the values of M_w determined by GPC and SEC-MALS-IV followed the same trends, although modified by a mentioned factor. Hereinafter, only SEC-MALS-IV data on the molecular weight of DCH materials will be discussed.

Outlined, besides the expected critical influence of $NaClO_2$ concentration on the molecular weight distribution of DCH, the duration of POX was revealed to significantly affect the M_w hand in hand with *DO*. The other sequential oxidation parameters exhibit rather moderate (t_{SOX}) or minor (HYA : $NaIO_4$ molar ratio) effects on the molecular weight of the resulting DCH, although significantly influencing other material properties such as *DO*. Finally, almost identical properties (namely M_w and *DO*) of the three DCH samples prepared using the same reaction conditions (A-DCH-02, B-DCH-04, and C-DCH-04) signify very good reproducibility of DCH synthesis. The following part focuses on the cytotoxicity of the selected prepared hyaluronate derivatives.

3.3 In vitro cytotoxicity

The cytotoxicity of the source HYA, DAH, the selected DCH samples, and sodium hyaluronate with comparable M_w (88 kDa, noted as HYA2) was evaluated using mouse embryonic fibroblasts cell line NIH/3T3, which represents immortalized healthy cells. Selected DCH samples were tested also on epithelial ovarian cancer cell line A2780 and compared with HYA2. The cytotoxicity was established by MTT assay after 48 h of treatment, see Section *2.5*. Results are given in Figure 4 and Figure S8; the red line in the figures represents the cell viability of 70% above which are compounds considered non-toxic according to ISO 10993-5.

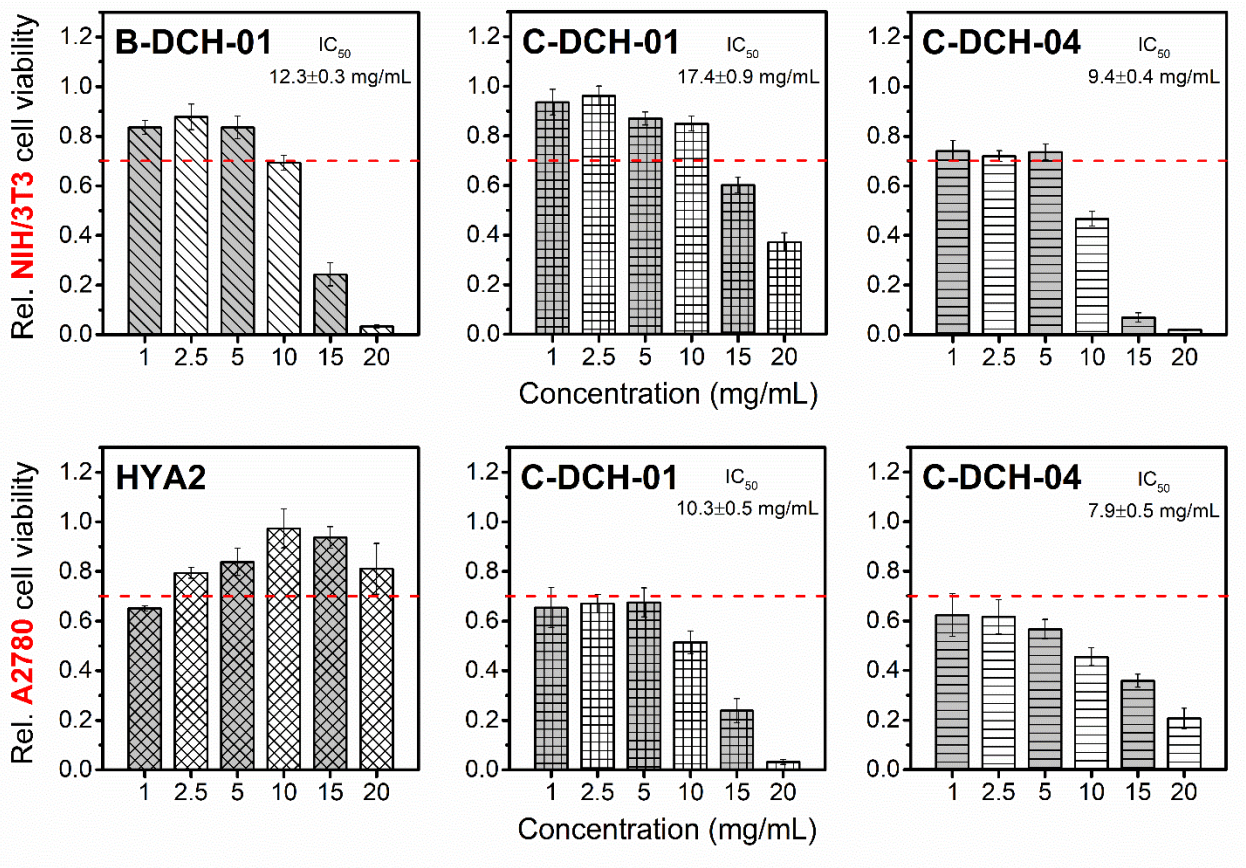

Figure 4 Relative cell viability of NIH/3T3 and A2780 cell lines 48 h after treatment with HYA2 and various DCH samples including IC_{50} values. The x-axis represents concentrations of compounds ranging from 1 to 20 mg/mL, the y-axis represents relative cell viability (%). Data are displayed as mean ± *SD*.

It is not surprising that untreated HYA and HYA2 did not exhibit any cytotoxicity towards NIH/3T3 (~100% relative cell viability even at the highest tested concentration of 20 mg/mL, Figure S8). On the other hand, DAH was by far the most cytotoxic compound with IC_{50}, a concentration of compound required to inhibit the cell growth of the cells by 50%, of 0.3 ± 0.1 mg/mL, which is more than an order of magnitude less (more cytotoxic) than tested DCH samples, likely due to its reactive aldehyde groups. Similarly, the B-DCH-01 sample (24 h POX, 4 h SOX) containing a large fraction of non-oxidized –CHO groups is significantly more cytotoxic (IC_{50} = 12.1 ± 0.3 mg/mL) than C-DCH-01 (4 h POX, 24 h SOX, IC_{50} =17.4 ± 0.9 mg/mL) with roughly 30% of unoxidized HYA GlcA units. Interestingly, the fully oxidized C-DCH-04 sample (complete POX and SOX) showed comparably higher cytotoxicity (IC_{50} = 9.4 ± 0.4 mg/mL) than the other two tested DCH samples. The reason is unclear, however, we speculate that this may not be (entirely) a result of its chemical composition, but also of its comparatively lower molecular weight (M_w = ~25 kDa) as low-molecular-weight HYA is associated with inflammation and other negative biological responses. (Misra et al., 2015) Some studies, however, suggest that these properties may be beneficial for cancer treatment. (Ghatak et al., 2002; Tavianatou et al., 2019) Therefore, the C-DCH samples were also tested against the A2780 cell line and compared with HYA2. Interestingly, HYA2 seems to negatively influence the A2780 cell

growth already at the lowest tested concentration (1 mg/mL), while higher concentrations seem to have minimal effect. This behavior was not observed for NIH/3T3, where the cell viability for the HYA2 sample was comparable to HYA (Figure S8 in SI). Notably, both C-DCH derivatives also showed borderline or moderate cytotoxicity towards A2780 already at 1 mg/mL, and exhibited IC_{50} values significantly lower than for NIH/3T3, namely 10.3 ± 0.5 mg/mL for C-DCH-01 and 7.9 ± 0.5 mg/mL for C-DCH-04. Both C-DCH derivatives thus demonstrate increased cytotoxicity towards malignant A2780 cell line compared to NIH/3T3 cell line, which may be beneficial for anticancer applications. Moreover, in a broader perspective, cytotoxicity of all tested DCH samples is several times lower than other previously investigated dicarboxylated polysaccharides, *i.e.* dicarboxycellulose, dicarboxydextran or dicarboxydextrin. (Münster, Fojtů, Capáková, et al., 2021)

3.4 DFT simulations, CP conjugation, and anticancer activity evaluation

To better illustrate structural differences between HYA and DCH, models containing three basic structural units (six monosaccharide units) were prepared *in silico* and optimized using DFT, see Figure 5, where the structure of the central unit of HYA/DCH is depicted in detail. The defining feature of HYA oxidation is the breaking of the bond between C2 and C3 and the repulsion of introduced –COOH groups, which increased the C2-C3 distance from ~1.5 Å to ~3.7 Å, Figure 5. The ring-opening then leads to additional changes in DCH chain conformation and an increased steric hindrance of –COOH at C6 by sidechains of neighboring GlcNAc units. For instance, the distance of C6 carbon atom from its closest neighbors, *i.e.* the $–CH_3$ group and C2-OH group from neighboring GlcNAc units, decreased after oxidation from ~4.5 and ~4.2 Å to only ~4.1 and ~3.3 Å, respectively, see space-fill models in Figure 5 for better illustration. The carboxyl groups at C6 of oxidized GclA units in DCH are thus less accessible than in HYA, which is more than compensated by an introduction of a pair of –COOH groups in positions C2 and C3.

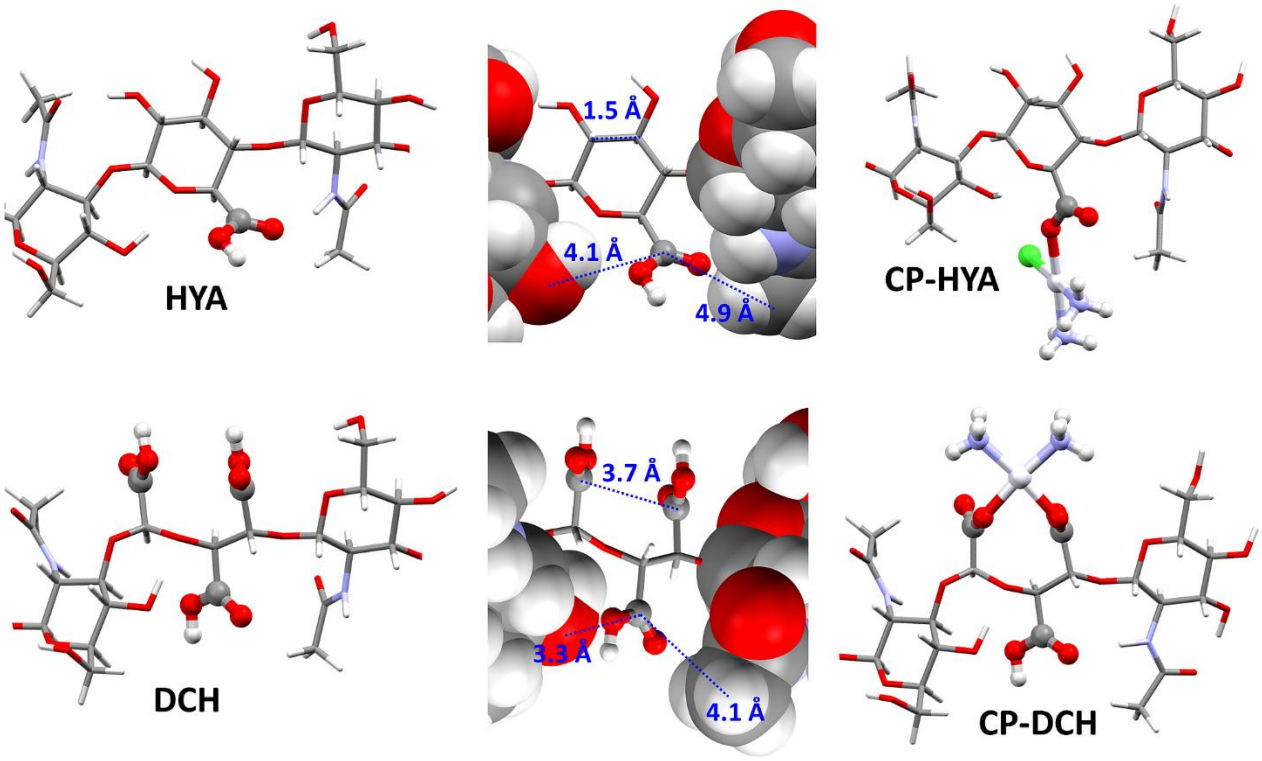

Figure 5 Detail of the DFT optimized structures of HYA and DCH with carboxyl groups emphasized by ball and stick model (left part); the steric hindrance of GlcA unit exemplified by a space-filling model with distances between C6 of GlcA and the $–CH_3$ group and C2-OH group of neighboring GlcNAc (center); the difference between the cisplatin (CP) binding modes (right).

To practically demonstrate the impact of differences between HYA and DCH structures, the leading anticancer drug CP was conjugated to HYA2 (M_w = 88 kDa), C-DCH-01 (*DO* = 70%, M_w = 57 kDa) and C-DCH-04 (*DO* = 99%, M_w = 25 kDa) samples. The conjugation reaction between CP and DCH is depicted in Scheme 2. Three different CP : carrier w/w ratios 2:10, 6:10, and 10:10 were employed. The conjugation of CP was investigated by IR spectroscopy, see Figure S9 for spectra of HYA2, C-DCH-04, and corresponding CP conjugates (10:10 w/w). Besides the appearance of *v*s vibration of NH_3 groups of CP (3270 cm^{-1}), the CP binding is confirmed by (i) a shift of asymmetric COO^- vibration from 1603 cm^{-1} to 1639 cm^{-1} for HYA2 and from 1608 cm^{-1} to 1638 cm^{-1} for C-DCH-04, (ii) by shifting and intensity increase of other bands associated with different vibrational modes of carboxyl groups (1390–1410 cm^{-1}). The CP binding to HYA2 caused a shift of the band around 1404 cm^{-1} to 1374 cm^{-1}, which is accompanied by an increase in intensity, while the CP binding to C-DCH-04 is accompanied by an even larger shift of the band at 1394 cm^{-1} to 1357 cm^{-1} and greater intensity increase, which reflects the discussed differences in CP binding between HYA2 and C-DCH-04. All of these changes are in line with expected CP binding to carboxyl groups of HYA and DCH.

Differences in conjugation efficacy and the amount of loaded drug in wt% (white-to-grey columns and orange-to-red columns, respectively) of the prepared conjugates were measured by XRF and are summarized in the top-left graph of Figure 6.

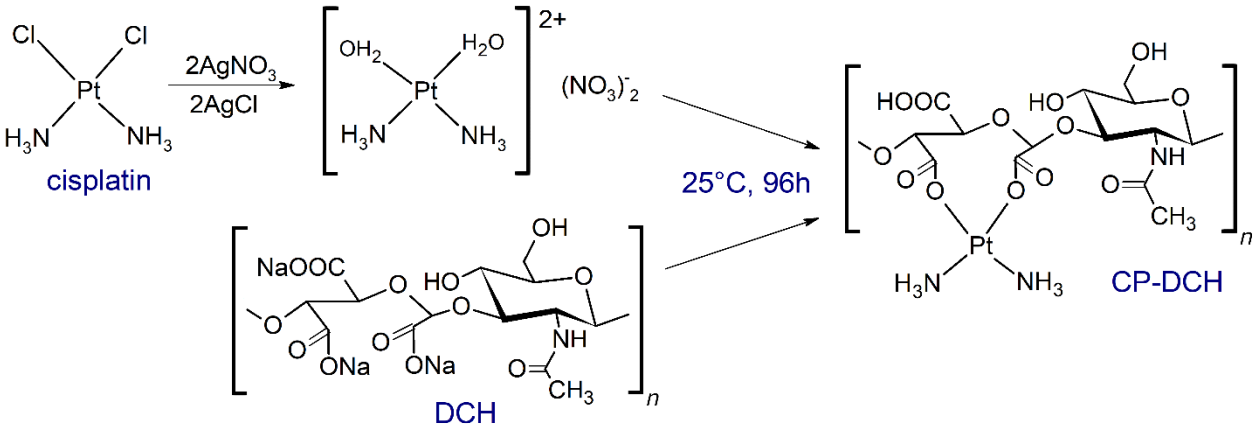

Scheme 2 Activation of cisplatin by $AgNO_3$ and subsequent conjugation reaction with DCH.

The presence of the easily accessible pair of –COOH groups in DCH samples, which are in an ideal position and orientation for chelation of metal centers, (Münster et al., 2019) resulted in significantly higher loading efficacy at higher reaction ratios compared to the HYA2 sample (59 *vs.* 44% for 10:10 ratio). In addition, while maximum CP content (loading capacity) in the CP-HYA2 sample did not exceed 28 wt% in agreement with previous reports, (Cai et al., 2008) the DCH could bind up to 53 wt% of CP. Interestingly, the decrease of *DO* to 70% led only to a relatively minor decrease of CP content (47 wt%) when using the highest loading ratio.

To further investigate differences between CP conjugation, CP binding modes were analyzed also on the DFT level. CP residues were introduced into optimized structures of HYA2 and DCH and these were re-optimized. Because CP can bind to HYA only *via* –COOH group in position C6 (Figure 5, right), two HYA units are required to saturate a single molecule of CP (only one is shown in Figure 5 to save computational time). The CP : HYA2 molar ratio is thus 0.5: 1, which corresponds to an observed maximum drug loading of 28 wt%, assuming M_{CP2+} = 227 g/mol and M_{HYA-} = 400 g/mol. The HYA2 is thus fully saturated already at a 6 : 10 reaction ratio. On the other hand, the easy accessibility of a pair of –COOH groups at C2 and C3 in DCH, together with increased steric protection of C6, results in a predominance of bidentate CP conjugation (Figure 5) as was recently experimentally confirmed. (Münster, Fojtů, Capáková, et al., 2021). The measured 53 wt% maximum drug loading for CP-DCH-04 is close to CP : DCH molar ratio 1:1 (58 wt%), assuming M_{CP2+} = 227 g/mol and M_{DCH2-} = 429 g/mol. Only when these primary binding sites are saturated, the monodentate CP binding at C6 is likely to occur. This is the case of CP-DCH-01, which features the same loading efficacy as fully-oxidized CP-DCH-04 for up to 6:10 w/w loading ratio, but maximal observed CP content at 10:10 loading ratio is decreased to 47 wt% due to monodentate CP binding to unoxidized units.

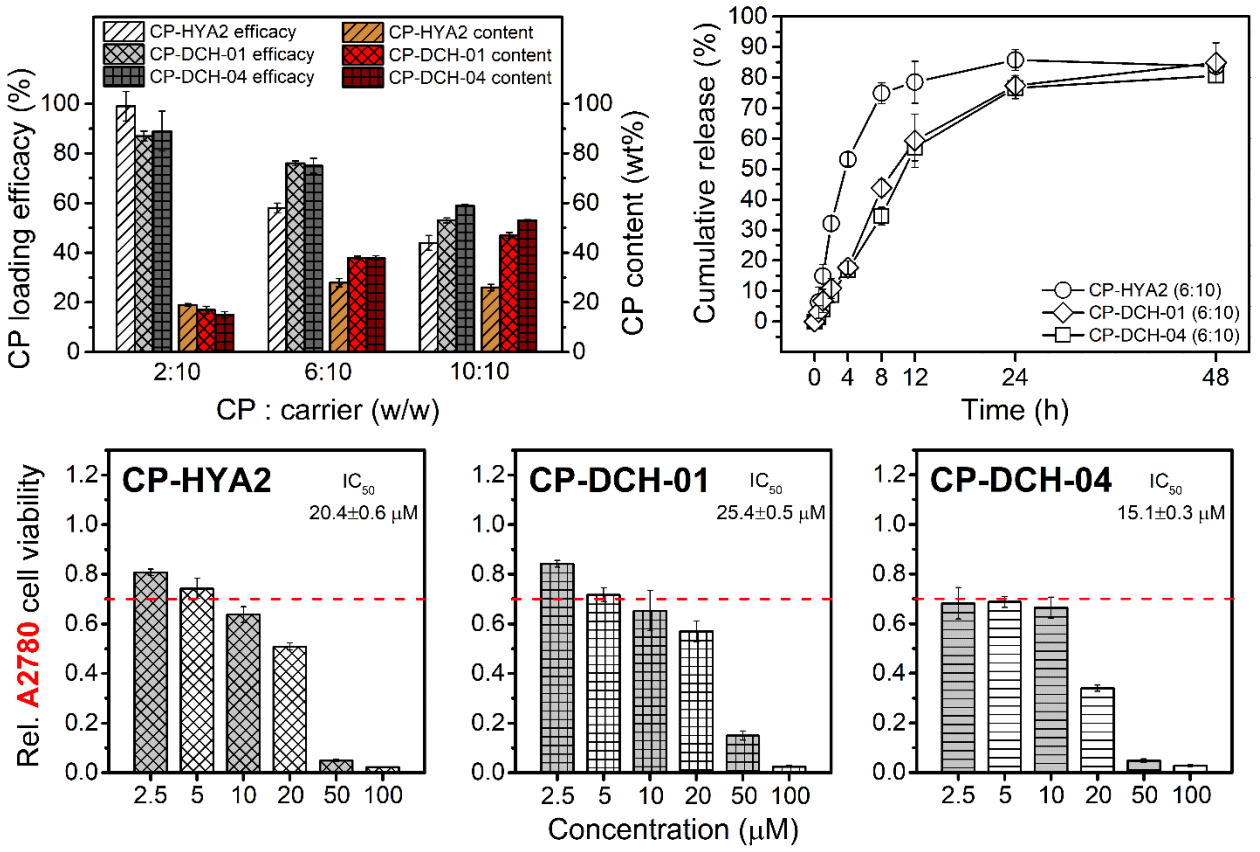

Figure 6 Top-left part – CP loading efficacy (%) and CP content (wt%) for CP-HYA2 and CP-DCH conjugates loaded using various CP : carrier w/w ratios (2:10, 6:10 and 10:10). Top-right part – Cumulative release of CP from CP-HYA2 and CP-DCH (both CP : carrier = 6:10 w/w). Bottom row – Cytotoxicity of the conjugates prepared using the 6:10 w/w loading ratio (CP : carrier) evaluated against malignant human ovarian cancer cell line A2780 with IC_{50} values. Data are displayed as mean ± *SD*. The lines connecting datapoints in the top right graph are only guides for the eyes.

The differences in CP binding are crucial for the drug release, as can be seen from a comparison of CP release rates from CP-DCH and CP-HYA2 conjugates loaded utilizing 6:10 w/w ratio of CP : carrier in the top-right graph of Figure 6. Despite lower drug content and higher M_w, the release of CP from HYA2 is significantly faster than from DCH derivatives. In two hours, over one-third of total CP is released from HYA2, compared to less than 10% in the case of DCH derivatives. After 8 hours, only between 35–40% of total CP is released from CP-DCH conjugates, while the release of CP from HYA2 is essentially finished. The gradual CP release kinetics of CP-DCH conjugates is another proof of the preferential bidentate CP binding in DCH. (Münster, Fojtů, Capáková, et al., 2021)

The comparatively higher CP loading efficacy, increased CP binding capacity, and gradual CP release renders DCH potentially very interesting for drug delivery applications. Besides, the DCH should be, at least theoretically, still capable of binding to CD44 or RHAMM receptors of HYA because the oxidation and the conjugation of CP residues in positions 2 and 3 do not interfere with receptor binding groups (the –COOH

group located at C6 of GlcA and the N-acetyl groups of GlcNAc units). (Dovedytis et al., 2020) Because these receptors are often overexpressed in numerous cancer cell lines, active tumor targeting may be possible.

Next, the anti-cancer activity of CP-DCH conjugates prepared using the 6:10 loading ratio was investigated using A2780 cell line and compared with CP-HYA2 (bottom row of graphs in Figure 6) as well as against healthy cell line NIH/3T3 (Figure S8). Note, that to compensate for different CP content in the conjugates, the doses of various samples were adjusted to contain the same amount of CP. The results thus directly reflect the potentiation/attenuation of CP therapeutic effect due to binding to the given carrier. While the IC_{50} of the conjugate for NIH/3T3 cell line were comparable within experimental error (Figure S8), CP-DCH-04 with IC_{50} = 15.1 ± 0.3 μM was significantly more effective than the CP-HYA2 with 20.5 ± 0.6 μM and the partially oxidized CP-DCH-01 with IC_{50} = 25.1 ± 0.5 μM. Conjugation to fully oxidized DCH thus potentiated the CP anticancer efficacy against A2780 compared to other conjugates. Additional studies, particularly *in vivo* assessments, which are beyond the scope of this work, are however required to unequivocally determine the full potential of DCH for anticancer drug delivery.

5. Conclusions

The study on the preparation of 2,3-dicarboxylated hyaluronate (DCH) was conducted concerning the variation of different synthesis parameters (oxidizing agent concentration, reaction time, molar ratio of reagents) of primary (POX) and secondary (SOX) oxidations. The effect of each parameter was evaluated using suitable analytical methods with the following findings:

(i) The concentration of sodium chlorite ($NaClO_2$) within SOX was found to significantly influence the DCH molecular structure, *i.e.* both the composition of functional groups and macromolecular properties such as molecular weight. The concentrations above 0.1 M of $NaClO_2$ exhibit a negative effect resulting in non-selective oxidation accompanied by the macromolecular chain degradation and thus should be avoided.

(ii) The shorter duration of SOX (below 12 h) leaves a significant amount of –CHO groups unoxidized, which negatively affects biocompatibility.

(iii) The duration of POX impacts both the *DO* and molecular weight. By the utilization of short POX, partially oxidized DCH composed of relatively large macromolecules (DP_w up to 128) can be prepared. Such materials exhibit lower cytotoxicity than fully oxidized DCH of comparably smaller molecular weight (DP_w up to 52).

(iv) The molar ratio of POX reagents was found to minorly influence the molecular weight of DCH products, but have a significant impact on *DO* when combined with shorter reaction times.

(v) The cytotoxicity of the tested partially and fully oxidized DCH samples towards NIH/3T3 cell line representing healthy cells is generally quite low and adverse effects on the cell viability appear only for very high doses >10 mg/mL. The DCH cytotoxicity is enhanced by the presence of residual –CHO groups (DAH is many times more cytotoxic than DCH), but also rises somewhat with increasing *DO*. Materials

partially oxidized in POX are thus the least cytotoxic. Moreover, unlike the NIH/3T3 cell line, the decrease of A2780 cell viability after incubation with DCH is observed even at the lowest tested concentration.

(vi) The comparative CP loading, release, and cytotoxicity study of CP-HYA2 and CP-DCH conjugates showed superior CP loading efficacy, greater loading capacity, and slower release kinetics of the DCH samples compared to unmodified HYA2. Moreover, the CP-DCH sample showed significantly higher cytotoxicity towards A2780 cell lines. Further studies including *in vivo* experiments are planned to confirm these results.

To summarize, given the well-defined structure, the presence of three –COOH groups per unit of DCH, and interesting anticancer efficacy, DCH derivatives are interesting not only for drug-delivery applications but also possess large modification potential which can be further exploited by the scientific community focusing on functional polysaccharide derivatization.

Acknowledgments

This work was supported by the Ministry of Education, Youth and Sports of the Czech Republic – DKRVO (RP/CPS/2022/007). Z. Capáková and P. Humpolíček acknowledge the Czech Science Foundation grant (20-28732S). CIISB research infrastructure project LM2018127 funded by the Ministry of Education, Youth and Sports of the Czech Republic is gratefully acknowledged for the financial support of the NMR measurements at the Josef Dadok CEITEC core facility in Brno. Computational resources were supplied by the project "e-Infrastruktura CZ" (e-INFRA CZ LM2018140) supported by the Ministry of Education, Youth and Sports of the Czech Republic.

Associated Information

Supplementary Information is available – FT-IR spectra of DCH series, DCH ^{1}H NMR and ^{1}H–^{13}C NMR correlation spectra, results of GPC and SEC-MALS-IV analyses of DCH samples.

Author Information

Author Contributions. **L. Münster:** synthesis and characterization of hyaluronate derivatives and conjugates, drug release study, writing of the manuscript; **Z. Capáková:** *in vitro* testing; **P. Humpolíček:** experimental design; **I. Kuřitka:** writing of the manuscript, experimental design; **B. E. Christensen:** writing of the manuscript, experimental design; **J. Vícha:** synthesis of cisplatin and conjugates, NMR measurements, DFT calculations, writing of the manuscript.

Notes

The authors declare no competing financial interest.

References:

Adamo, C., & Barone, V. (1999). Toward reliable density functional methods without adjustable parameters: The PBE0 model. *The Journal of Chemical Physics*, *110*(13), 6158–6170. https://doi.org/10.1063/1.478522

Andrae, D., Häußermann, U., Dolg, M., Stoll, H., & Preuß, H. (1990). Energy-adjustedab initio pseudopotentials for the second and third row transition elements. *Theoretica Chimica Acta*, *77*(2), 123–141. https://doi.org/10.1007/BF01114537

Balazs, E. A. (1992). Medical Applications of Hyaluronan and its Derivatives. In T. Cheng, C. G. Gebelein, & V. C. Yang (Eds.), *Cosmetic and Pharmaceutical Applications of Polymers*. Springer. http://public.eblib.com/choice/PublicFullRecord.aspx?p=6489820

Bayer, I. S. (2020). Hyaluronic Acid and Controlled Release: A Review. *Molecules*, *25*(11), 2649. https://doi.org/10.3390/molecules25112649

Cai, S., Xie, Y., Bagby, T. R., Cohen, M. S., & Forrest, M. L. (2008). Intralymphatic Chemotherapy Using a Hyaluronan–Cisplatin Conjugate. *Journal of Surgical Research*, *147*(2), 247–252. https://doi.org/10.1016/j.jss.2008.02.048

Cyphert, J. M., Trempus, C. S., & Garantziotis, S. (2015). Size Matters: Molecular Weight Specificity of Hyaluronan Effects in Cell Biology. *International Journal of Cell Biology*, *2015*, 1–8. https://doi.org/10.1155/2015/563818

Deng, Y., Ren, J., Chen, G., Li, G., Wu, X., Wang, G., Gu, G., & Li, J. (2017). Injectable in situ cross-linking chitosan-hyaluronic acid based hydrogels for abdominal tissue regeneration. *Scientific Reports*, *7*(1), 2699. https://doi.org/10.1038/s41598-017-02962-z

Dovedytis, M., Liu, Z. J., & Bartlett, S. (2020). Hyaluronic acid and its biomedical applications: A review. *Engineered Regeneration*, *1*, 102–113. https://doi.org/10.1016/j.engreg.2020.10.001

Fallacara, A., Baldini, E., Manfredini, S., & Vertuani, S. (2018). Hyaluronic Acid in the Third Millennium. *Polymers*, *10*(7), 701. https://doi.org/10.3390/polym10070701

Felgueiras, H. P., Wang, L. M., Ren, K. F., Querido, M. M., Jin, Q., Barbosa, M. A., Ji, J., & Martins, M. C. L. (2017). Octadecyl Chains Immobilized onto Hyaluronic Acid Coatings by Thiol–ene "Click Chemistry" Increase the Surface Antimicrobial Properties and Prevent Platelet Adhesion and Activation to Polyurethane. *ACS Applied Materials & Interfaces*, *9*(9), 7979–7989. https://doi.org/10.1021/acsami.6b16415

Fraser, J. R. E., Laurent, T. C., & Laurent, U. B. G. (1997). Hyaluronan: Its nature, distribution, functions and turnover. *Journal of Internal Medicine*, *242*(1), 27–33. https://doi.org/10.1046/j.1365-2796.1997.00170.x

Fu, S., Dong, H., Deng, X., Zhuo, R., & Zhong, Z. (2017). Injectable hyaluronic acid/poly(ethylene glycol) hydrogels crosslinked via strain-promoted azide-alkyne cycloaddition click reaction. *Carbohydrate Polymers*, *169*, 332–340. https://doi.org/10.1016/j.carbpol.2017.04.028

Ghatak, S., Misra, S., & Toole, B. P. (2002). Hyaluronan Oligosaccharides Inhibit Anchorage-independent Growth of Tumor Cells by Suppressing the Phosphoinositide 3-Kinase/Akt Cell Survival Pathway. *Journal of Biological Chemistry*, *277*(41), 38013–38020. https://doi.org/10.1074/jbc.M202404200

Girish, K. S., & Kemparaju, K. (2007). The magic glue hyaluronan and its eraser hyaluronidase: A biological overview. *Life Sciences*, *80*(21), 1921–1943. https://doi.org/10.1016/j.lfs.2007.02.037

Grimme, S. (2006). Semiempirical GGA-type density functional constructed with a long-range dispersion correction. *Journal of Computational Chemistry*, *27*(15), 1787–1799. https://doi.org/10.1002/jcc.20495

Kim, H., Shin, M., Han, S., Kwon, W., & Hahn, S. K. (2019). Hyaluronic Acid Derivatives for Translational Medicines. *Biomacromolecules*, *20*(8), 2889–2903. https://doi.org/10.1021/acs.biomac.9b00564

Knopf-Marques, H., Pravda, M., Wolfova, L., Velebny, V., Schaaf, P., Vrana, N. E., & Lavalle, P. (2016). Hyaluronic Acid and Its Derivatives in Coating and Delivery Systems: Applications in Tissue Engineering, Regenerative Medicine and Immunomodulation. *Advanced Healthcare Materials*, *5*(22), 2841–2855. https://doi.org/10.1002/adhm.201600316

Kristiansen, K. A., Dalheim, M. Ø., & Christensen, B. E. (2013). Periodate oxidation and macromolecular compaction of hyaluronan. *Pure and Applied Chemistry*, *85*(9), 1893–1900. https://doi.org/10.1351/pac-con-13-01-05

Kristiansen, K. A., Potthast, A., & Christensen, B. E. (2010). Periodate oxidation of polysaccharides for modification of chemical and physical properties. *Carbohydrate Research*, *345*(10), 1264–1271. https://doi.org/10.1016/j.carres.2010.02.011

Larrañeta, E., Henry, M., Irwin, N. J., Trotter, J., Perminova, A. A., & Donnelly, R. F. (2018). Synthesis and characterization of hyaluronic acid hydrogels crosslinked using a solvent-free process for potential biomedical applications. *Carbohydrate Polymers*, *181*, 1194–1205. https://doi.org/10.1016/j.carbpol.2017.12.015

Laurent, T. C. (Ed.). (1998). *The chemistry, biology, and medical applications of hyaluronan and its derivatives*. Portland Press.

Maia, J., Carvalho, R. A., Coelho, J. F. J., Simões, P. N., & Gil, M. H. (2011). Insight on the periodate oxidation of dextran and its structural vicissitudes. *Polymer*, *52*(2), 258–265. https://doi.org/10.1016/j.polymer.2010.11.058

Marchessault, R. H., Ravenelle, F., & Zhu, X. X. (Eds.). (2006). *Polysaccharides for Drug Delivery and Pharmaceutical Applications* (Vol. 934). American Chemical Society. https://doi.org/10.1021/bk-2006-0934

Metaxa, A.-F., Vrontaki, E., Efthimiadou, E. K., & Mavromoustakos, T. (2021). Drug Delivery Systems Based on Modified Polysaccharides: Synthesis and. In T. Mavromoustakos, A. G. Tzakos, & S.

Durdagi (Eds.), *Supramolecules in Drug Discovery and Drug Delivery* (Vol. 2207, pp. 151–161). Springer US. https://doi.org/10.1007/978-1-0716-0920-0_12

Misra, S., Hascall, V. C., Markwald, R. R., & Ghatak, S. (2015). Interactions between Hyaluronan and Its Receptors (CD44, RHAMM) Regulate the Activities of Inflammation and Cancer. *Frontiers in Immunology*, *6*. https://doi.org/10.3389/fimmu.2015.00201

Muchová, M., Münster, L., Vávrová, A., Capáková, Z., Kuřitka, I., & Vícha, J. (2022). Comparison of dialdehyde polysaccharides as crosslinkers for hydrogels: The case of poly(vinyl alcohol). *Carbohydrate Polymers*, *279*, 119022. https://doi.org/10.1016/j.carbpol.2021.119022

Münster, L., Fojtů, M., Capáková, Z., Muchová, M., Musilová, L., Vaculovič, T., Balvan, J., Kuřitka, I., Masařík, M., & Vícha, J. (2021). Oxidized polysaccharides for anticancer-drug delivery: What is the role of structure? *Carbohydrate Polymers*, *257*, 117562. https://doi.org/10.1016/j.carbpol.2020.117562

Münster, L., Fojtů, M., Capáková, Z., Vaculovič, T., Tvrdoňová, M., Kuřitka, I., Masařík, M., & Vícha, J. (2019). Selectively oxidized cellulose with adjustable molecular weight for controlled release of platinum anticancer drugs. *Biomacromolecules*, *20*(4), 1623–1634. https://doi.org/10.1021/acs.biomac.8b01807

Münster, L., Fojtů, M., Muchová, M., Latečka, F., Káčerová, S., Capáková, Z., Juriňáková, T., Kuřitka, I., Masařík, M., & Vícha, J. (2021). Enhancing cisplatin anticancer effectivity and migrastatic potential by modulation of molecular weight of oxidized dextran carrier. *Carbohydrate Polymers*, *272*, 118461. https://doi.org/10.1016/j.carbpol.2021.118461

Münster, L., Hanulíková, B., Machovský, M., Latečka, F., Kuřitka, I., & Vícha, J. (2020). Mechanism of sulfonation-induced chain scission of selectively oxidized polysaccharides. *Carbohydrate Polymers*, *229*, 115503. https://doi.org/10.1016/j.carbpol.2019.115503

Münster, L., Vícha, J., Klofáč, J., Masař, M., Kucharczyk, P., & Kuřitka, I. (2017). Stability and aging of solubilized dialdehyde cellulose. *Cellulose*, *24*(7), 2753–2766. https://doi.org/10.1007/s10570-017-1314-x

Pandit, A. H., Mazumdar, N., & Ahmad, S. (2019). Periodate oxidized hyaluronic acid-based hydrogel scaffolds for tissue engineering applications. *International Journal of Biological Macromolecules*, *137*, 853–869. https://doi.org/10.1016/j.ijbiomac.2019.07.014

Pawlak, T., Niedzielska, D., Vícha, J., Marek, R., & Pazderski, L. (2014). Dimeric Pd(II) and Pt(II) chloride organometallics with 2-phenylpyridine and their solvolysis in dimethylsulfoxide. *Journal of Organometallic Chemistry*, *759*, 58–66. https://doi.org/10.1016/j.jorganchem.2014.02.016

Ponedel'kina, I. Y., Khaibrakhmanova, E. A., Tyumkina, T. V., Romadova, I. V., & Odinokov, V. N. (2015). Stoichiometric C6-oxidation of hyaluronic acid by oxoammonium salt TEMPO + Cl − in an aqueous alkaline medium. *Carbohydrate Polymers*, *130*, 69–76. https://doi.org/10.1016/j.carbpol.2015.04.054

Prasher, P., Sharma, M., Mehta, M., Satija, S., Aljabali, A. A., Tambuwala, M. M., Anand, K., Sharma, N., Dureja, H., Jha, N. K., Gupta, G., Gulati, M., Singh, S. K., Chellappan, D. K., Paudel, K. R., Hansbro, P. M., & Dua, K. (2021). Current-status and applications of polysaccharides in drug delivery systems. *Colloid and Interface Science Communications*, *42*, 100418. https://doi.org/10.1016/j.colcom.2021.100418

Schanté, C. E., Zuber, G., Herlin, C., & Vandamme, T. F. (2011). Chemical modifications of hyaluronic acid for the synthesis of derivatives for a broad range of biomedical applications. *Carbohydrate Polymers*, *85*(3), 469–489. https://doi.org/10.1016/j.carbpol.2011.03.019

Shan, J., Böck, T., Keller, T., Forster, L., Blunk, T., Groll, J., & Teßmar, J. (2021). TEMPO/TCC as a Chemo Selective Alternative for the Oxidation of Hyaluronic Acid. *Molecules*, *26*(19), 5963. https://doi.org/10.3390/molecules26195963

Shanmuga Doss, S., Bhatt, N. P., & Jayaraman, G. (2017). Improving the accuracy of hyaluronic acid molecular weight estimation by conventional size exclusion chromatography. *Journal of Chromatography B*, *1060*, 255–261. https://doi.org/10.1016/j.jchromb.2017.06.006

Sharma, A. K., Prasher, P., Aljabali, A. A., Mishra, V., Gandhi, H., Kumar, S., Mutalik, S., Chellappan, D. K., Tambuwala, M. M., Dua, K., & Kapoor, D. N. (2020). Emerging era of "somes": Polymersomes as versatile drug delivery carrier for cancer diagnostics and therapy. *Drug Delivery and Translational Research*, *10*(5), 1171–1190. https://doi.org/10.1007/s13346-020-00789-2

Sieger, D., Korzinskas, T., Jung, O., Stojanovic, S., Wenisch, S., Smeets, R., Gosau, M., Schnettler, R., Najman, S., & Barbeck, M. (2019). The Addition of High Doses of Hyaluronic Acid to a Biphasic Bone Substitute Decreases the Proinflammatory Tissue Response. *International Journal of Molecular Sciences*, *20*(8), 1969. https://doi.org/10.3390/ijms20081969

Sirviö, J. A., Liimatainen, H., Visanko, M., & Niinimäki, J. (2014). Optimization of dicarboxylic acid cellulose synthesis: Reaction stoichiometry and role of hypochlorite scavengers. *Carbohydrate Polymers*, *114*, 73–77. https://doi.org/10.1016/j.carbpol.2014.07.081

Smith, L. J., Taimoory, S. M., Tam, R. Y., Baker, A. E. G., Binth Mohammad, N., Trant, J. F., & Shoichet, M. S. (2018). Diels–Alder Click-Cross-Linked Hydrogels with Increased Reactivity Enable 3D Cell Encapsulation. *Biomacromolecules*, *19*(3), 926–935. https://doi.org/10.1021/acs.biomac.7b01715

Tavianatou, A.-G., Piperigkou, Z., Barbera, C., Beninatto, R., Masola, V., Caon, I., Onisto, M., Franchi, M., Galesso, D., & Karamanos, N. K. (2019). Molecular size-dependent specificity of hyaluronan on functional properties, morphology and matrix composition of mammary cancer cells. *Matrix Biology Plus*, *3*, 100008. https://doi.org/10.1016/j.mbplus.2019.100008

Toole, B. P. (2004). Hyaluronan: From extracellular glue to pericellular cue. *Nature Reviews Cancer*, *4*(7), 528–539. https://doi.org/10.1038/nrc1391

Turley, E. A., Noble, P. W., & Bourguignon, L. Y. W. (2002). Signaling Properties of Hyaluronan Receptors. *Journal of Biological Chemistry*, *277*(7), 4589–4592. https://doi.org/10.1074/jbc.R100038200

Vigetti, D., Karousou, E., Viola, M., Deleonibus, S., De Luca, G., & Passi, A. (2014). Hyaluronan: Biosynthesis and signaling. *Biochimica et Biophysica Acta (BBA) - General Subjects*, *1840*(8), 2452–2459. https://doi.org/10.1016/j.bbagen.2014.02.001

Vold, I. M. N., & Christensen, B. E. (2005). Periodate oxidation of chitosans with different chemical compositions. *Carbohydrate Research*, *340*(4), 679–684. https://doi.org/10.1016/j.carres.2005.01.002

Vold, I. M. N., Kristiansen, K. A., & Christensen, B. E. (2006). A Study of the Chain Stiffness and Extension of Alginates, in Vitro Epimerized Alginates, and Periodate-Oxidized Alginates Using Size-Exclusion Chromatography Combined with Light Scattering and Viscosity Detectors. *Biomacromolecules*, *7*(7), 2136–2146. https://doi.org/10.1021/bm060099n

Weigend, F., & Ahlrichs, R. (2005). Balanced basis sets of split valence, triple zeta valence and quadruple zeta valence quality for H to Rn: Design and assessment of accuracy. *Physical Chemistry Chemical Physics*, *7*(18), 3297. https://doi.org/10.1039/b508541a

Weis, M., Shan, J., Kuhlmann, M., Jungst, T., Tessmar, J., & Groll, J. (2018). Evaluation of Hydrogels Based on Oxidized Hyaluronic Acid for Bioprinting. *Gels*, *4*(4), 82. https://doi.org/10.3390/gels4040082

Wilson, J. J., & Lippard, S. J. (2014). Synthetic Methods for the Preparation of Platinum Anticancer Complexes. *Chemical Reviews*, *114*(8), 4470–4495. https://doi.org/10.1021/cr4004314